

Characteristics of tropical cyclone precipitation features over the western Pacific warm pool

Levi Thatcher,¹ Yukari N. Takayabu,² Chie Yokoyama,¹ and Zhaoxia Pu¹

Received 16 December 2011; revised 9 July 2012; accepted 10 July 2012; published 18 August 2012.

[1] In this study, ten years (1998–2007) of the Tropical Rainfall Measuring Mission (TRMM)-derivative radar precipitation feature (PF) product are analyzed in order to determine the differences between tropical cyclone-related precipitation characteristics compared with those of the tropical Pacific warm pool (10 to 30°N and 130 to 150°E) in general. The PF data, from the University of Utah's archive, are based on the TRMM precipitation radar's 2A25 product, where one PF consists of a single or group of contiguous pixels with near surface rainfall greater than zero. Using the PF database, the height and area of tropical background PFs versus those within 500 km of tropical cyclones (TCs) are compared. It is found that TC-related PFs are markedly more frequent from 5 to 10 km altitude than are background tropical PFs. The enhanced midlevel TC-related populations not only exist in stratiform precipitation around the melting level at 5.5 km, but also from 6 to 9 km in stratiform regions, in convective precipitation, and when culling the smallest features from the data set. This increase in congestus-like echoes in TC environments aligns well with observations regarding mesoscale convective systems (MCSs), in which the enhanced ice present in MCS (and TC) environments creates a stabilized melting layer through cooling immediately below 0°C. This stable layer appears to enhance the detrainment of convective PFs in our TC data set at and for a few kilometers above the melting level.

Citation: Thatcher, L., Y. N. Takayabu, C. Yokoyama, and Z. Pu (2012), Characteristics of tropical cyclone precipitation features over the western Pacific warm pool, *J. Geophys. Res.*, 117, D16208, doi:10.1029/2011JD017351.

1. Introduction

[2] Due to a lack of systematic atmospheric observations over the tropical oceans, many phenomena related to tropical cyclones (TCs) have never been sufficiently explained. The processes related to such storms' intensity changes, in particular, have proved quite vexing [Wang and Wu, 2004; Halverson *et al.*, 2007]. For example, forecasts of TC intensity change have only been improving roughly 1.1% per year since 1990 [Rogers *et al.*, 2006]. Among the various uncertainties related to TC intensity change, there are still important gaps in our understanding of TC clouds and precipitation characteristics. This is despite the important fact that TC rapid intensity changes often occur in conjunction with the rapid reorganization of the cyclones' cloud and precipitation structures. These structures are essential not only to our understanding of TC relevant processes, but also because of

their impact on the numerical simulations of these storms [Houze, 2010].

[3] While the amount of work that has been done related to tropical precipitation distributions is substantial, the literature regarding the differences between TC and tropical precipitation is still somewhat limited. Even into the 1960s, basic views of the tropical distribution of clouds were still rare. The overall early lack of data was finally addressed in the 1970s by the Marshall Island and Global Atmospheric Research Program Atlantic Tropical Experiments (GATE), which focused on determining the general characteristics of tropical convection. Many studies used GATE sounding data and found much evidence of widespread shallow trade cumulus, which have been defined as being below 4 km [Johnson *et al.*, 1999], and deep cumulonimbus clouds, or a bimodality in large scale tropical convection [Yanai *et al.*, 1973; Schubert, 1976; Randall and Huffman, 1980]. While Yanai *et al.* [1976] found some unexplained midlevel detrainment in the Marshall Island experiments, using GATE data, Houze and Cheng [1977] found an abundance of midlevel clouds. In fact, using data from the 5.3 cm radar on the *Oceanographer*, they found that 60% of radar-echo tops fell between 4 km and 9 km height, which contradicted previous general notions that tropical clouds were largely comprised of shallow cumulus and tall cumulonimbus clouds.

[4] Studies related to the Tropical Ocean Global Atmosphere Coupled Ocean Atmosphere Response Experiment

¹Department of Atmospheric Sciences, University of Utah, Salt Lake City, Utah, USA.

²Atmosphere and Ocean Research Institute, University of Tokyo, Tokyo, Japan.

Corresponding author: L. Thatcher, Department of Atmospheric Sciences, University of Utah, 135 S 1460 E, Rm. 819, Salt Lake City, UT 84112, USA. (levi.thatcher@utah.edu)

(TOGA-COARE) in 1992–1993 further refined the tropical cloud modality question using ship-based radar and sounding data. *Rickenbach and Rutledge* [1998], using data from MIT's C-band Doppler radar aboard the R/V *Vickers*, found that most convective rainfall for all event types was associated with deep (14–15 km) convection, with a secondary maximum of features at 8–10 km height. *Johnson et al.* [1999] later expanded upon these findings and, using the same TOGA-COARE C-band data, found that “cumulus congestus clouds are the most abundant of all precipitating clouds in COARE.” Specifically, they determined that congestus, with tops between 4.5 and 9.5 km (which is how this paper will define them), represents 57% of the precipitating convective clouds and 28% of the total rainfall in COARE [*Johnson et al.*, 1999]. Similarly, the contribution to rainfall was 30% for echo tops between 4 and 9 km in GATE [*Cheng and Houze*, 1979]. With the help of a couple well-designed field experiments and a careful analysis of the data, over two decades the overall view of tropical clouds went from being based around a simple bimodality between cumulus and cumulonimbus, to one that considers congestus as providing a significant fraction of the total distribution.

[5] Cumulus congestus often form because of the increased detrainment taking place around the stable, 0°C melting layer. This was documented by *Johnson et al.* [1996, 1999], who used TOGA-COARE data to study temperature and moisture perturbations near the 0°C level over the west Pacific warm pool. Surprisingly, for what was known at the time, they determined that one-half of their analyzed soundings displayed recognizable stable layers within ~100 hPa of the 0°C layer. They went on to state that stable layers near the 0°C level were nearly as common as trade wind stable layers over the warm pool. *Johnson et al.* [1999] further explained that the sub-melting-level cooling occurred primarily near MCSs and other precipitating systems, which suggests they are primarily a result of melting within stratiform rain regions. However, the presence of this effect in TCs has not been detailed.

[6] Considering the difficulty inherent in producing accurate TC intensity forecasts and the current uncertainties involved in the relevant parameterizations, it is essential to properly understand TC cloud populations and their interactions with the TC thermodynamic environment.

[7] A number of field campaigns (such as IFEX and Camex-3 and 4) have collected dropsondes in TC environments [*Franklin et al.*, 2003; *Rogers et al.*, 2006], however, there are only a limited number of TCs per field campaign. Meanwhile, sondes are often dropped below the freezing level. Because of these and other considerations, most of the sonde-based studies of TC thermodynamic profiles have been case studies. Very few studies of such profiles include statistics from a large number of cyclones. Furthermore, there have also been few attempts to analyze, using a large number of TCs, the unique features of TC-related precipitating clouds as compared to those in the general tropics. While such studies were not possible in the past, over the last decade a large number of TCs have been observed by the Tropical Rainfall Measuring Mission (TRMM), such that this type of analysis is now possible.

[8] The purpose of the current paper is to examine if, and how, TC-related precipitation feature characteristics differ from general tropical precipitation features. This is done using

10 years of TRMM precipitation radar data over the west Pacific warm pool region. Using the University of Utah's precipitation feature (PF) database and Joint Typhoon Warning Center (JTWC) best track data, the resultant TC PF data is compared to that of the tropical Pacific in terms of its frequency and rainfall contribution by both PF height and area.

[9] Section 2 of this paper briefly describes TRMM's precipitation radar (PR) and the resultant precipitation feature database housed at the University of Utah. The methods used to facilitate the comparison between tropical versus TC-related features are here explained. Section 3 includes a discussion of the results. Section 4 summarizes this study and addresses the implications for future research.

2. Data and Methods

[10] The data used in this study are from TRMM's precipitation radar (PR). This PR was the first radar in space and was designed to provide a vertical distribution of rainfall over the tropics. It operates at 13.8 GHz and has a horizontal and vertical resolution of 4.3 km and 250 m, respectively [*Kummerow et al.*, 1998]. TRMM's PR suffers from significant attenuation and thus, to produce estimates of rainfall, it is necessary to correct for this before radar echo power is converted into rainfall rates [*Iguchi et al.*, 2000]. The TRMM product which performs this correction is the 2A25. According to *Iguchi et al.* [2000], the 2A25 product “estimates the true effective reflectivity factor Z_e at 13.8 GHz at each radar resolution cell from the measured vertical profiles of reflectivity factor Z_m ” after which the rainfall rate is calculated from the estimated Z_e . Further, the rainfall estimates are made from the Z_e profiles by using the power law $R = aZ_e^b$, where a and b are both “functions of the rain type and the heights of the 0°C isotherm and storm top” [*Iguchi et al.*, 2000]. In general, the 13.8 GHz radar is sensitive to rain stronger than 0.7 mm hr⁻¹ (at 16–18 dBZ [*Kozu et al.*, 2001]), but is not sensitive to drizzle or small cloud ice [see *Smith et al.*, 1997]. Because of this, echo top often does not equal cloud top; the distance between these two heights depends on the type of cloud involved. If the convection is weak then the distance can be large, but if the convection is very strong then the echo-versus-cloud top distance can be negligible. Many convective systems have large (i.e., visible to the PR) ice particles aloft, but, indeed, for those echoes that are not associated with strong updrafts and large ice particles, the echo top height could be underestimating the actual height by a few kilometers [*Liu et al.*, 2007].

[11] Based on the enormous amount of data the PR made available, precipitation features (PFs) were created as a simple way to summarize precipitation events in a coherent manner [*Nesbitt et al.*, 2000; *Cecil et al.*, 2005]. The radar precipitation features (which we subsequently call PFs) used in this study are from the University of Utah archive, which are defined such that one feature consists of a set of contiguous PR 2A25 Version 6 pixels, with near-surface rainfall rate greater than zero [*Liu et al.*, 2008]. Through this method, the original information of pixel-level measurements is compressed into the characteristics of features and better summarizes the information of an observed event [*Liu et al.*, 2008]. PF height is simply the height of its highest pixel; this method was chosen because this height generally is a proxy of the maximum intensity of the convection in the

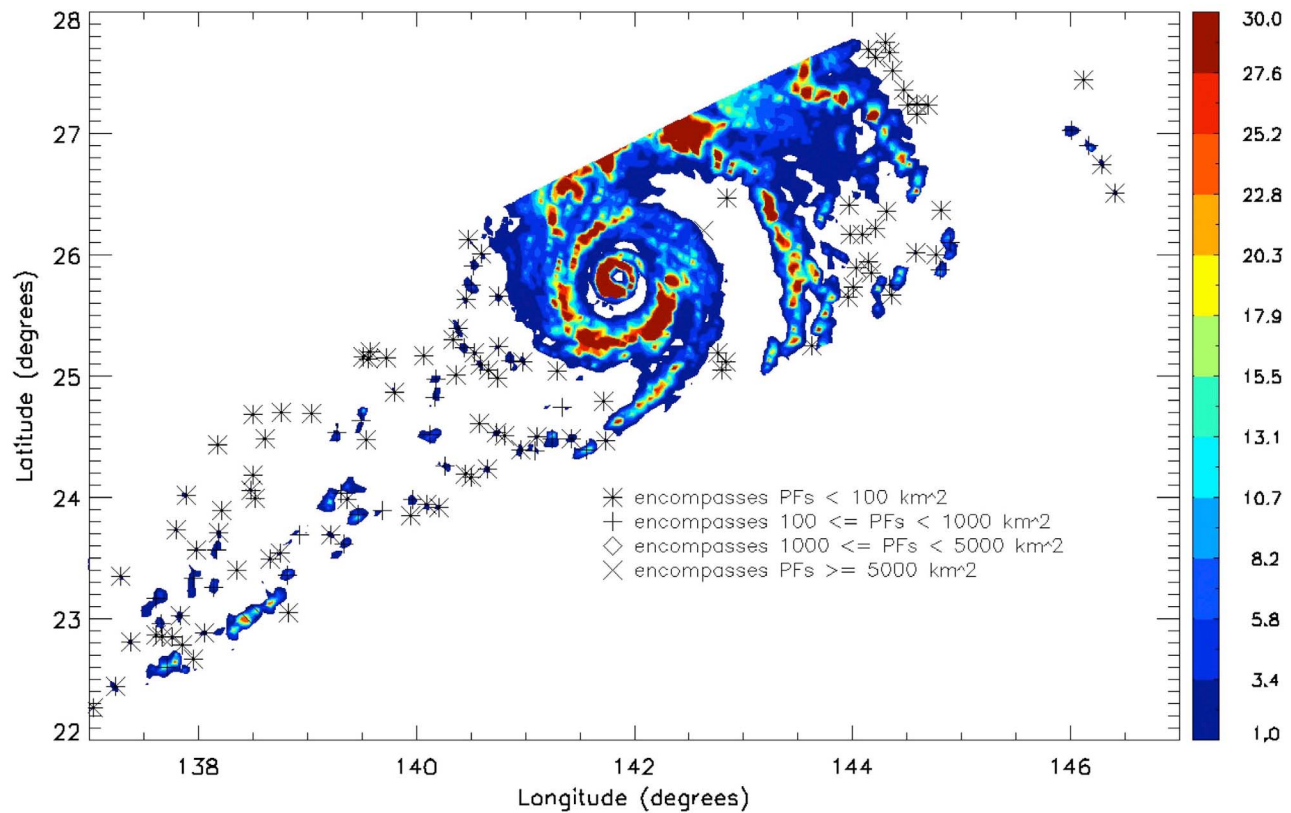


Figure 1. View of both near-surface 2A25 rainfall rate (mm hr^{-1}) and accompanying precipitation features near Typhoon Kajiki (2007) from TRMM orbit number 56574 at 1702 UTC 20 October 2007.

system. Precipitation features are created even for a single 2A25 pixel and these are assigned an area of 17.92 km^2 before, and 20.35 km^2 after, the TRMM altitude boost which occurred in August 2001. While, indeed, some of these single pixel PFs may arise due to radar returns from questionable artifacts, in aggregate they do contain a significant amount of information. In this study, of the PFs found in the specified warm pool region (see next paragraph), 46.0% were composed of only one pixel. Of the TC-related PFs, 50.5% were composed of only one pixel. This is not only a characteristic of TRMM's PR either, as *Johnson et al.* [1999], in their survey of results from TOGA-COARE, noted that 95% (80%) of their convective features were less than 25 (15) km in length.

[12] A specific portion of the western Pacific warm pool region (i.e., $130\text{--}150^\circ\text{E}$ longitude and $10\text{--}30^\circ\text{N}$ latitude) was chosen as the focus of the study because of the frequency with which TCs form over this vast expanse of water. The years 1998–2007 were chosen, as this period encompasses a full decade and provides a significant amount of TC-related PF data. In this study, TC tracks are obtained from the best track data as archived by the JTWC. All TC best track data in JTWC's collection during the ten year period are used without regard to storm intensity. In terms of the comparisons between TC precipitation features and tropical precipitation features, we generally focus on discussing and organizing the PFs in terms of height and area, following *Yokoyama and Takayabu* [2012].

[13] First, combing the PF database for features of all sizes that fall within the area and timeframe of interest, a data set consisting of 1,853,813 west Pacific precipitation features is created. In order to enable the comparison between west Pacific tropical PFs in general and those associated with TC activity, another data set is constructed, similarly to what was done by *Jiang et al.* [2011]. This process is such that only PFs occurring within 500 km of the TC center are considered, as defined by the JTWC best track for all geographically relevant storms from 1998 to 2007. The database includes nascent as well as decaying tropical storms, thus providing not only precipitation features in TCs themselves, but also in environments conducive to, and associated with, their presence. We must also emphasize here that, considering the much higher amount of area included when encompassing large radii, PFs here categorized as being TC-related will typically be part of either the inner or outer rainbands or further from the center. Only the occasional TC PF will represent an eyewall.

[14] The 6-hourly JTWC best-track data is linearly interpolated and made hourly to enable a higher temporal resolution when deciding which PFs are deemed as TC-related. With these constraints our TC PF data set includes 81,105 PFs, which had been situated in the vicinity of 216 different TCs. As only 9 TCs worldwide during this 10 year period had been completely missed by TRMM, the data provides a comprehensive view of west Pacific TC precipitation features. To provide an example, Figure 1 shows the distribution of PFs around Typhoon Kajiki (2007) and the

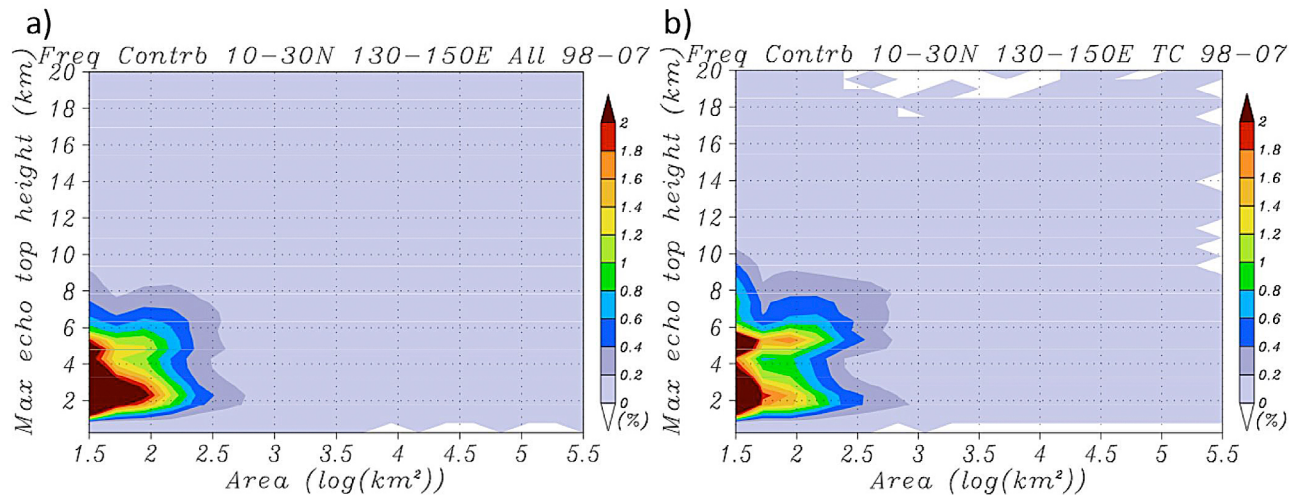


Figure 2. Comparison of frequency distribution (in percentage terms) of (a) tropical PFs and (b) TC-related PFs in terms of their area (km^2) and echo top height (km). The period is 1998–2007 and the spatial coverage is 130–150°E and 10–30°N.

accompanying 2A25 near-surface (1–1.5 km) hourly rainfall rate. The domain of this figure is large enough to provide a view of how PFs scatter around TCs and background tropical environments. The binning of PFs by area in this figure provides a useful way to visualize how rainfall associated with TCs can largely be summarized into just a few precipitation features. By contrast, the areas further from the TC demonstrate how the majority of background PFs are composed of just a few pixels. Some of the PFs composed of just one pixel are not always accompanied by a noticeable rainfall amount (Figure 1).

[15] In order to determine the confidence level at which we can say that these TC PF features differ from those in the west Pacific general tropical environment, the two-sample Kolmogorov-Smirnov (KS2) test is used. This test assumes as its null hypothesis that the two data sets are from the same distribution and accordingly determines the probability of these two data sets randomly occurring. This probability is expressed as the p-value. The KS2 test is appropriate here considering the fact that it is a nonparametric method and our data has a decidedly non-Gaussian distribution. Given the null hypothesis that the TC PF height and general tropical height data would fall within the same distribution, according to the KS2 test the p-value is zero. In other words, the probability of these two data sets both occurring, while they are both from the same distribution, is zero. The corresponding test for PF area yielded a p-value of zero as well. In terms of both height and area, it is thus safe to proceed with the knowledge that the differences between west Pacific TC PFs and tropical PFs are statistically significant. The actual practical importance of this will be discussed in the next section.

3. Results and Discussion

[16] The two separate PF data sets, obtained from the aforementioned procedures, can now be discussed in terms of the differences in their area and height distribution characteristics. Recall that these PFs are composed of at least one pixel of near-surface rainfall and are categorized by echo top

height. Figure 2 shows the frequency distribution, in percentage terms, of the two sets of PFs by height and area. It appears that both TC and tropical PFs (subsequently referred to as either features, echoes, or PFs) are predominately small and short in terms of frequency. Specifically, it is apparent that TC environments exhibit a larger population of PFs reaching 5.5 km height, and out to an area of 315 km^2 , compared with the west Pacific. There is also a significant decrease in echoes whose tops are from 1 to 4 km height and out to around 125 km^2 in area in TC-related PFs. These patterns are found to persist throughout the 10 year period. This is also seen in Figure 3, wherein the simple frequency distribution by PF height and size is shown for each year from 1999 to 2003. Despite the complications of the TRMM boost in August 2001, there is a consistent and marked increase in 5.5 km high PFs in TCs as compared to the general west Pacific. This difference is thus deemed not only statistically significant, but also practically significant, as it is readily seen when a comparison is made for only a modest amount of TCs.

[17] While there is a local maxima in echo frequency in both data sets around 5.5 km (where PFs from 5 to 10 km here will be defined as being cumulus congestus-like), the TC-related PFs are even more concentrated there. This supports Johnson *et al.*'s idea that MCSs and similar storms tend to exacerbate the accompanying melting level stable layer. Essentially, the heightened amount of snow and ice in MCS-like environments will, through melting and cooling below 0°C, induce a well-developed stable layer [Zuidema, 1998; Johnson *et al.*, 1999] that can persist for days, such that these stable layers can be remnants of preexisting convection [Johnson *et al.*, 1996]. In order to demonstrate the mechanism behind this stable layer, Figure 4 reproduces Figure 14 from Johnson *et al.* [1996]. The figure composited TOGA-COARE soundings having lapse rates less than 5°C km^{-1} “over a 20-mb-deep layer within 50 mb of the 0°C level” into four bins depending on the level of relative humidity from 400–700 hPa; these four groupings of soundings represent 60% of all 1745 IOP soundings analyzed. For each bin the relevant data were displayed on a

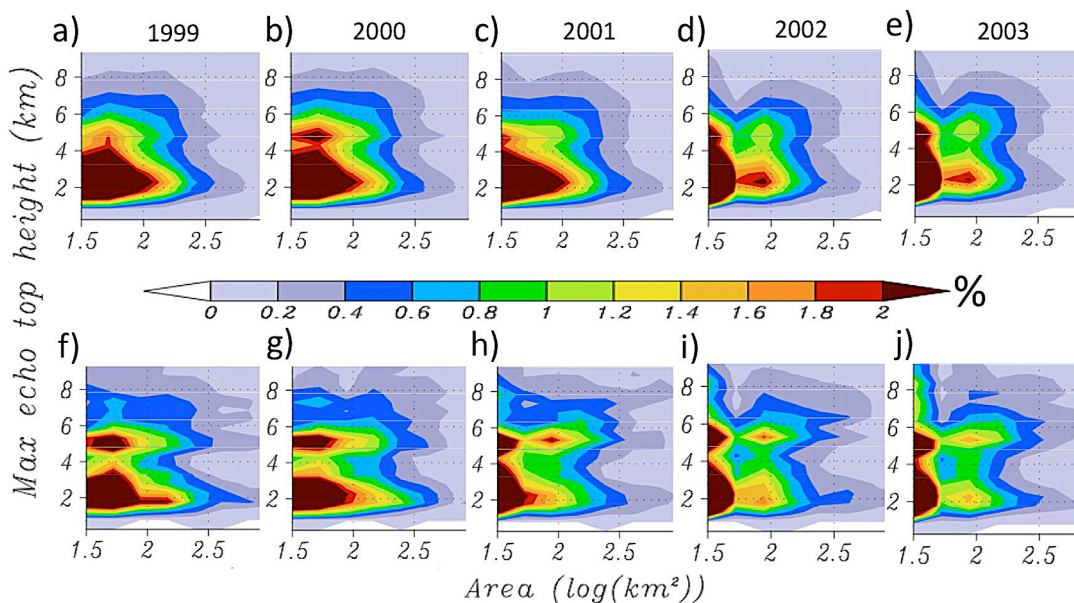


Figure 3. Yearly frequency distribution in terms of PF area (km^2) and echo top height (km) for the (a–e) west Pacific tropical and (f–j) TC environments. These years are selected to show the robustness of the pattern despite the impact of the TRMM boost in 2001.

skew-T log P diagram. The figure demonstrates that, in TOGA-COARE environments with stable layers, the soundings with more moisture from 400 to 700 hPa were also cooler slightly below the 600 hPa melting level. Thus this figure not only shows the typical thermodynamic profiles associated with 0°C stable layers, but also helps illustrate the fact that when stable layers form they often appear to be explained by the melting of hydrometeors, which could easily cause the associated cooling and moistening.

[18] Modeling studies [Ferrier and Houze, 1989; Taylor and Baker, 1991] have demonstrated that cloud detrainment occurs preferentially into these layers of higher static stability, corresponding to the number of echoes found at and above the melting layer.

[19] In addition to the slightly enhanced TC PF population extending to around 5.5 km (Figure 2), there is the aforementioned decrease in PFs between 1 and 4 km and out to an area of $10^{2.1} \text{ km}^2$, which indicates that TC environments are not only conducive to the generation of congestus-like echoes, but also associated with a marked decrease in shallow echoes. Considering the boundary layer and low-level mesoscale organization associated with TCs, this TC PF decrease below 5.5 km is not a surprise. Comparing the two aforementioned distributions to a PF oceanic background distribution from 10°S to 10°N and 155 to 175°E (not shown), it appears that the heightened low-level moisture around the equator, by decreasing low-level stability, inhibits low-level detrainment and the formation of 2–4 km (which we will call shallow) PF populations, similar to what happens within TC environments (Figure 2). Thus, the reduced amount of shallow PFs near TCs appears not only due to storm and feature organization, but also to differences in moisture between the semi-dry subtropical (10 – 30°N) environment and moist TCs. While this is expected, the quantification of this effect over such a large sample and with this level of detail is rarely seen in studies of tropical convection.

[20] In order to view these discrepancies in echo top height with a different, and more intuitive perspective, Figure 5 shows PF heights in a histogram for both west Pacific tropical and TC environments. To control for significantly different PF size distributions between the general tropics and TC environments, only those PFs composed of at least two pixels and with an area smaller than 1000 km^2 have been considered. This yields 40,182 TC and 1,000,704 background tropical features. Readily apparent is the increase in TC PFs, compared to the background tropics, around 5.5 km and the relative decrease around 2.5 km. Especially notable is the sharpness of this peak at 5.5 km. It thus appears that in TC environments the most common type of echo is that which occurs at and just above the melting level.

[21] Although the relative contributions from the increase in the amount of high echoes and the decrease in low echoes is difficult to determine from Figure 5, this is remedied by examining a cumulative distribution function (CDF) of the same data, which is shown in Figure 6. Perhaps most prominent is the aforementioned decrease in TC-related PFs, compared to the west Pacific tropics, from 2 to 5 km. This is followed by a sharp increase in TC-related features above 5 km which exists until roughly 10 km. While Figure 5 would make it seem that the TC-related 0°C stable layer causes the TC-only PFs to mostly appear around 5–6 km, this is not the case. One should note the fact that the cumulative probability of TC precipitation features at 5.8 km (Figure 6) is still notably lower than that of the tropics in general, but by 10 km the cumulative distributions are again roughly equal, indicating a much larger relative amount of TC features (as compared to the tropics) present from 6 to 10 km. Above 10 km TC and tropical PF heights have similar cumulative distributions.

[22] To determine whether these TC-only midlevel features are appearing in mostly stratiform or convective environments, we narrow the TC and tropical data sets into stratiform

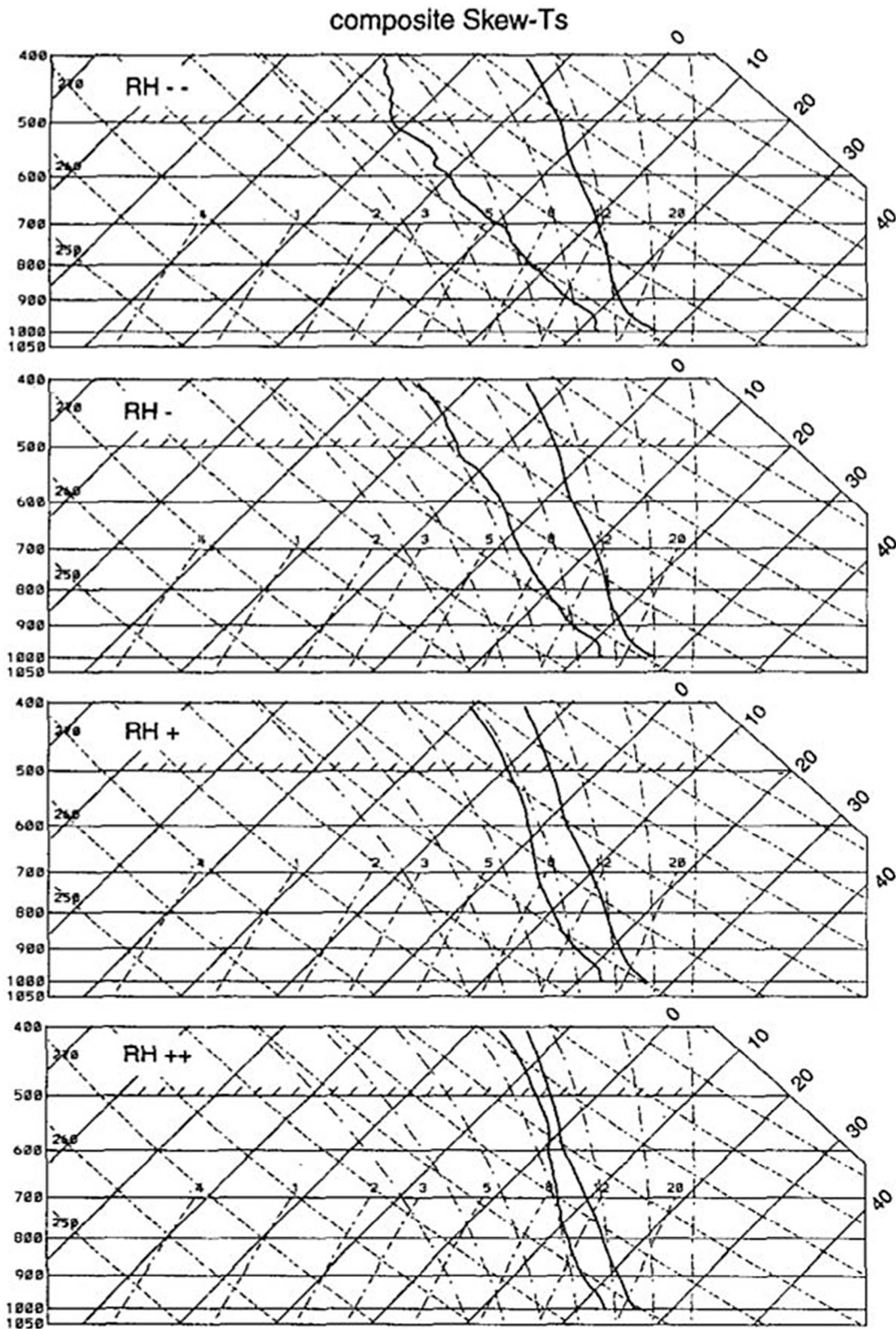


Figure 4. Composite profiles of TOGA-COARE soundings having lapse rates less than $5^{\circ}\text{C km}^{-1}$ “over a 20-mb-deep layer within 50 mb of the 0°C level” on skew-T log P diagrams for four relative humidity categories [from *Johnson et al.*, 1996, Figure 14] (© American Meteorological Society. Reprinted with permission.) To stratify the soundings by RH category, the average RH in the 400–700 hPa layer was compared against the time mean RH for that layer and then the four RH bins were defined using standard deviation thresholds. RH ++ represents the bin with the most moisture. See *Johnson et al.* [1996] for details.

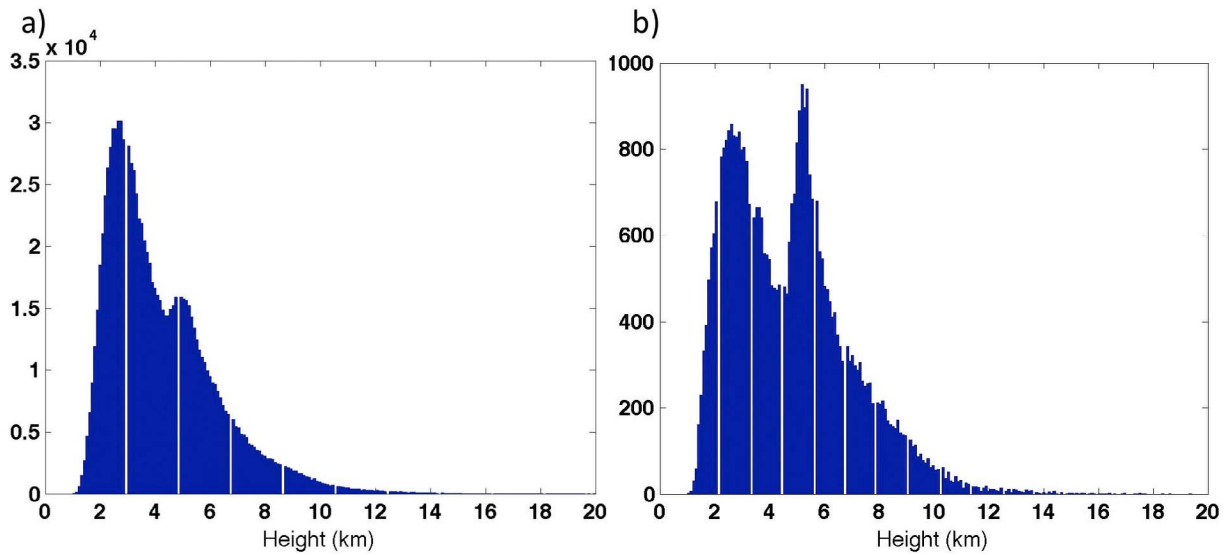


Figure 5. Histograms of PF heights over the 10 year period for (a) tropical PFs and (b) TC-related PFs. The vertical white lines in the figure are artifacts of the somewhat discretized height levels. To control for differences between tropical and TC environments, only PFs with at least two pixels and areas smaller than 1000 km² are considered.

and convective components, by selecting only those PFs that are either zero or 100 percent in terms of the PF stratiform rain ratio. TRMM’s 2A23 algorithm for determining whether rain is stratiform or convective was developed by *Awaka et al.* [1997], and is based around the vertical structure and horizontal variability of the echo [see *Steiner et al.*, 1995;

Schumacher and Houze, 2003b]. To further view the impact of PF size on these distributions, the data sets were also sorted in terms of PFs having a minimum of one or two pixels. Convective (stratiform) TC PFs of two or more pixels amount to 11,522 (14,367) features, whereas the background tropical convective (stratiform) count is 365,301 (294,093). This not

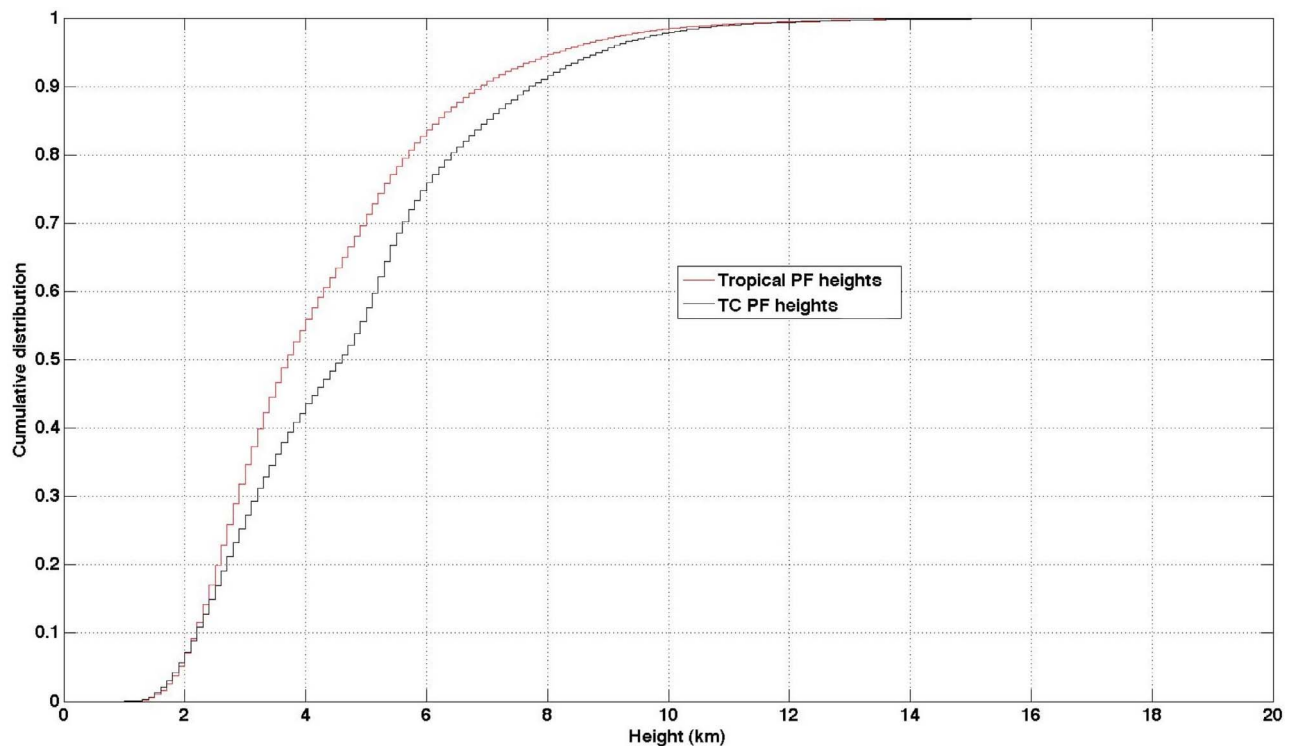


Figure 6. Cumulative distribution function (CDF) of PF heights for the west Pacific tropical atmosphere (red) and west Pacific TC environments (black). To control for differences between tropical and TC environments, only PFs with at least two pixels and areas smaller than 1000 km² are considered.

only demonstrates the depth of the data sets, but also the fact that, compared to the tropics, TC environments are decidedly more stratiform than convective, as indicated by *Yokoyama and Takayabu* [2008]. We must note that of the 40,182 TC PFs of at least two pixels and less than 1000 km² in area, 28.7% are deemed convective and 35.8% are deemed stratiform, which leaves an even greater category of PFs as being a mix between the two. Considering this and the difficulties present in making the stratiform/convective classification, this breakdown is only useful to explore the general behavior of PFs at either end of the precipitation type spectrum. The details of this split thus admittedly paint only a partial picture of what is actually happening in TC and tropical midlevel environments.

[23] These data are plotted in Figure 7 with PFs of all sizes (Figure 7a) and PFs of two or more pixels (Figure 7b). This figure generally shows that, despite the differences in detail, both convective and stratiform types of features are more prevalent from 5.5 to 10 km in TC environments as compared to the west Pacific in general. This is seen in the fact that the black lines catch up to the red lines, in terms of cumulative distribution, somewhere between 5.5 and 10 km. Notice that for stratiform rain this holds for both Figures 7a and 7b, and thus shows that the pattern is generally the same when culling the smallest PFs from the data set. This stratiform result demonstrates that stable-layer induced convective detraining only explains part of the mechanism behind the differences between TC and tropical PFs. For *both* types of precipitation, we also notice that, despite the number of parcels reaching around 5.5 km (and thus being recorded at that height), many of the TC-only PFs reach 6–9 km. The fact that so many convective echoes appear affected by the melting level may shed light on the duration of these stable layers, as the stability is created in largely stratiform regions [*Johnson et al.*, 1996].

[24] While some may question the ability of both stratiform and convective environments to produce temperature profiles conducive to these congestus-like PFs, there are many plausible scenarios describing how such thermal structures might exist. For example, *Leary and Houze* [1979] noted that stratiform cloud systems often have their bases around 0°C, partially due to cooling by melting, which causes downward acceleration below that level (Figure 4). *Johnson et al.* [1996] explained that this is not a rare phenomenon, as isothermal layers are “known to exist just below the melting level in stratiform rain regions.” *Warner et al.* [1980] also noted that the 0°C stable layer caused “considerable stratiform debris” near the 5 km level. Thus, while dry adiabatic layers in convective and stratiform environments may often occur, the stable layers described here are a well-documented phenomenon in both types of rainfall. Separately from these arguments, one should also expect enhanced stratiform PF populations in the midlevels of TCs, as compared to the tropics, because of the higher amount of mesoscale organization present in TC environments.

[25] The act of removing the smallest pixels from the data sets notably affects convective PF distributions. In the data set which included the smallest PFs (Figure 7a), roughly 90 (80) percent of convective tropical (TC) PFs are below 4 km. This difference appears entirely gone by 10 km. By contrast, when removing the smallest PFs, the differences in cumulative convective (TC versus tropical) counts by 4 km is

much smaller (Figure 7b). The convergence of two-pixel or more PFs in this convective distribution that is complete by 10 km is subsequently much smaller as well, which means a large amount of the congestus differences between TC and tropical convective PFs occurs in small features. Interestingly, the congestus differences between convective tropical and TC PFs greater than a pixel in size appear mainly to occur from 7 to 9 km in height (Figure 7b). To be clear, we are looking at slope differences in the figure, and the cumulative TC versus tropical “catch up” in two-plus pixel convective PFs occurs at that height.

[26] We interpret this to mean that the enhanced 0°C stable layer in TC environments first detrains the smallest parcels around 5.5 km, after which the effect is not present (for all sizes) from 5.8 to 6.3 km. Only above this height, from roughly 7 to 9 km, are the larger convective TC features detrained (Figure 7b). Note that from 7 to 9 km there is also a significant amount of one-pixel TC convective parcels detraining (Figure 7a). This may mean that the 0°C stable layer in TC environments is not strong enough to detrain, near 5–6 km, all of the smallest features nor hardly any of the features composed of two or more pixels. Since most of the differences between TC and tropical congestus occur at PF sizes of around 100 km² (Figure 3), here we are describing isolated convective elements represented by just a few pixels instead of those sustaining large, dynamic clouds. Considering this and the fact that we have no information on draft size, we assume the updraft-to-PF size ratio for these echoes to be relatively constant, in order to enable a discussion of the likely mechanism behind the varying PF sizes. The fact that the bigger parcels appear to finish detraining higher up generally confirms the fidelity of the data and aligns with *Johnson et al.*'s [1999] theory. However, we have no explanation for the lull present in part a) in terms of TC cumulative convective “catch-up” from 5.8 to 6.3 km (notice the change in concavity in the solid black line), but note that the phenomenon is very small in percentage terms.

[27] In terms of the vertical distribution between cumulus congestus and cumulonimbus clouds, a key role is played by the glaciation of parcels which do not detrain near the melting level. It has been hypothesized that vigorous updrafts which carry substantial amounts of supercooled cloud and rainwater well above the melting level achieve an extra boost of buoyancy due to the subsequent release of latent heat of fusion. These parcels often accelerate and achieve maximum updraft speed above 10 km [*Heymsfield et al.*, 2010] and form part of the deep cumulonimbus clouds that detrain at or near the tropopause. The presence of such cumulonimbus, tropical stratiform precipitation [*Schumacher and Houze*, 2003a], and congestus just above the melting level is well explained [*Johnson et al.*, 1999]. Less explained, however, is the presence of clouds with tops from 7 to 9 km (Figures 2 and 7a), which appear little affected by the stability at the much lower melting level (E. Zipser, personal communication, 2011). These type of clouds are well represented in this study by PFs with areas mostly less than 50 km² and from 7 to 9 km height (Figure 2). While the data here presented cannot shed substantial light on the mechanisms behind the presence of the small features extending to 7–9 km, it should be noted that they are more prevalent in TC environments, and that their size in this environment is more commonly confined to less than 50 km² when compared with the general

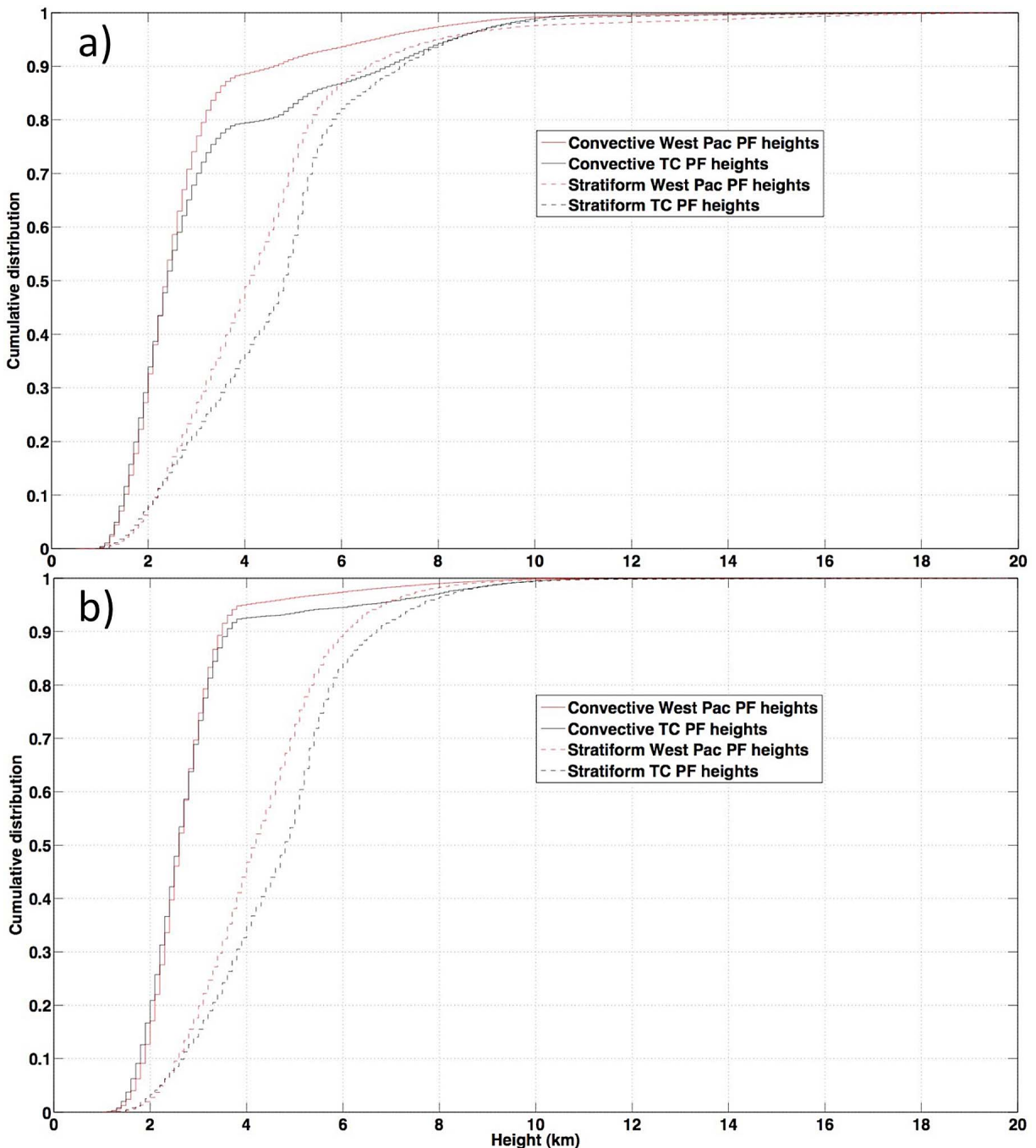


Figure 7. Cumulative distribution functions (CDF) of PF heights for (a) all PFs less than 1000 km^2 in area and (b) PFs less than 1000 km^2 in area containing at least two pixels. Red solid (dashed) lines represent convective (stratiform) west Pacific background PFs, whereas black solid (dashed) lines represent convective (stratiform) TC-related PFs. Stratiform (convective) features are those whose PF rain type category equals 100 percent (0 percent).

west Pacific. We speculate that these PFs could be a product of growing or decaying deep convection or may be due to a problem in observation, when echoes at this height may result from the TRMM PR partially capturing weak maritime cells which barely make it to the tropopause. An additional explanation may be that the TCs in which these 7–9 km PFs form may have notable dry layers that inhibit deep convection.

[28] After *Johnson et al.* [1999] explained the trimodal distribution of tropical clouds, several studies examined the possible role of moisture in limiting the depth of tropical convection [*Sherwood, 1999; Takemi et al., 2004; Takayabu et al., 2006; Jensen and Del Genio, 2006; Takayabu et al., 2010*]. Since there is a significant distance of many TC-only 7–9 km PFs from the melting level around 5.5 km, it appears that in a number of TCs, a midlevel dry layer could

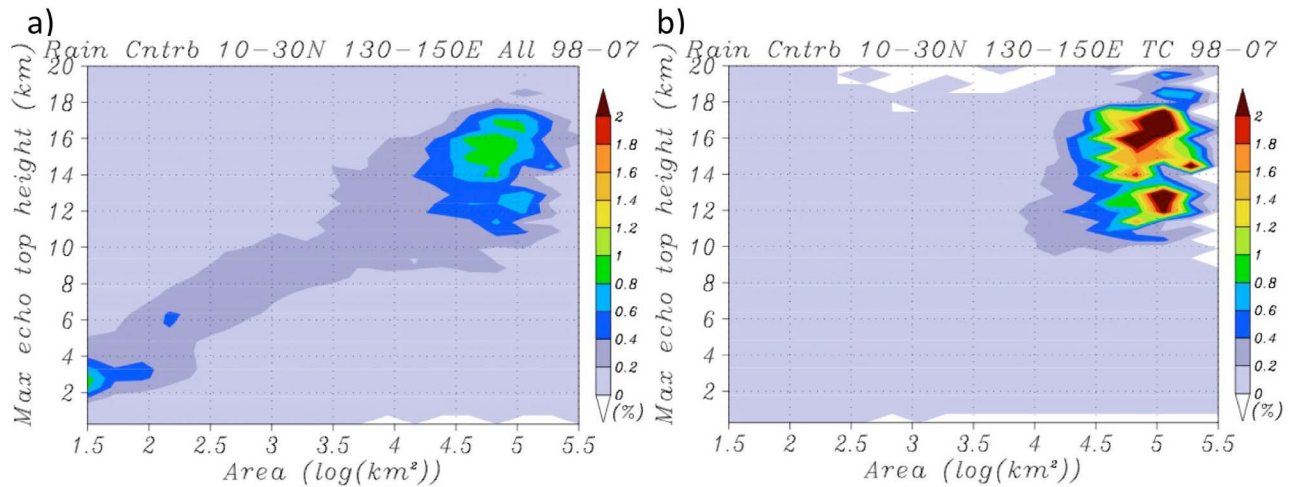


Figure 8. Comparison of PF rainfall contribution distributions (in percentage terms) of (a) tropical PFs and (b) TC-related PFs in terms of area (km²) and echo top height (km).

be inhibiting convection from reaching the tropopause. While many of the studies that analyzed the importance of dry layers in inhibiting convection found a noteworthy relationship, a number of them [Sherwood, 1999; Takemi et al., 2004; Jensen and Del Genio, 2006; Takayabu et al., 2006] still acknowledged that the melting-induced 0°C stable layer plays an important role in inhibiting cumulonimbus formation. Because of this, and the narrow concentration of TC-only congestus around 0°C (Figure 5), Johnson et al.'s [1999] explanation for the differences between tropical and TC-only congestus can be applied to our study.

[29] To view PF differences in terms of their contribution to rainfall, total rainfall distributions are calculated and presented in Figure 8. It is apparent that while most of the PFs in the West Pacific are small and short (Figures 2a and 2b), those that produce significant amounts of rainfall are tall (i.e., above 10 km) and large (i.e., over 10,000 km²). This result agrees with Houze and Cheng [1977]. In addition, significant differences are found between the distributions of heavy rain-bearing precipitation features in the Pacific tropical environment and those in the TCs of the region.

[30] Recall that many of the TC-related congestus-like PFs, which are ubiquitous at, and start around, 5 km, are markedly more common than in the general tropics up to 9 km (Figure 6). From Figure 8, it is evident that these TC-related congestus-like PFs contribute very little rainfall to the total amount present in TC environments. While tropical environments (Figure 8a) receive non-negligible amounts of rain from small shallow and larger congestus echoes up to around 8 km, the vast majority of TC-related rainfall comes from organization typified by deep stratus and cumulonimbus echoes above 10 km (Figure 8b). This concentration of TC rainfall into fewer echoes is expected, partially because of the structural organization present in TCs and the fact that most of these storms have tops near the tropopause. The extent to which this occurs, and its quantification, is, however, notable. A contributing factor could be that University of Utah PF data is constructed such that if the highest contiguous pixel is at, for example, 18 km height, the PF will be counted as occurring at that height. Thus, more organized rainfall leads to higher PFs. Despite these factors, many weak TCs are not

well organized and are composed of disparate cloud features, some of which we expected to have a maximum height from 5 to 9 km, providing a non-negligible amount of rain; overall, this midlevel contribution does not occur (Figure 8b). Finally, examining these TC and tropical rainfall distributions by year (not shown), we find that these particular patterns for shallow, midlevel, and upper-level PFs hold over relatively small samples of data.

4. Concluding Remarks

[31] To investigate the differences between West Pacific tropical PFs in general and tropical cyclone-related PFs, 10 years of TRMM precipitation radar data have been analyzed. It was found that, in TC environments, congestus-like (5–10 km height) radar echoes occur significantly more frequently than they do in the general west Pacific tropical environment. The increase in TC-related congestus is most notable around the 5–6 km height level, but exists up to around 10 km and is persistent throughout the 10 year sample (Figures 2, 3, 5, and 6). This difference is thought to be due to enhanced levels of ice in TC environments, the enhanced stabilized melting level, and the subsequent near-0°C-level cloud-capping detrainment that occurs. Johnson et al. [1999] suggested similar reasons for enhanced congestus populations in MCS environments, but did not examine this melting-stabilization mechanism with a sample of data containing many TC environments. We speculate that TC-only PFs from 7 to 9 km are partially due to slower total detrainment of larger parcels and are also occasionally affected by midlevel dry layers which inhibit convection from reaching the tropopause.

[32] While one would expect the melting-related 0°C stable layer to affect TC-related echoes in stratiform regions around 0°C, these enhanced populations not only exist in stratiform precipitation around 5.5 km, but also in convective precipitation regions (displaying stable layer longevity) and when culling the smallest features from the data set. The marked increase of midlevel clouds in TC versus background environments holds for yearly samples throughout the 1998–2007 period. It should be noted that, because of the nature of

the 500 km radial constraint, the large majority of the TC PFs are from (and outside of) the inner and outer rainbands, while only the occasional echo represents an eyewall.

[33] When studying PF patterns by rain type, it is found that convective PF distributions change significantly after stratifying for PF size. Essentially, the smallest convective TC-only features appear to detrain mostly around 5.5 and 7–9 km, whereas the larger TC-only convective PFs detrain solely from 7 to 9 km. Therefore, the smallest features detrain most quickly, whereas the PFs of at least two pixels detrain at least one kilometer above the 0°C level. As expected, stratiform echoes do not show the same height-area changes in TC and background populations as convective features, but rather have similar relative TC and background distributions whether they possess one or more pixels.

[34] While it was expected that large and deep features in TCs would account for a large part of the total rainfall, despite the enhanced *congustus* populations it was found that essentially all TC-related rainfall comes from PFs larger than 10,000 km² and with echo tops above 10 km.

[35] Although this had been studied previously, this paper goes beyond prior studies by quantifying TC and tropical PF frequency and rainfall differences, by height, over an extensive sample.

[36] By proxy, this study provides a picture of midlevel thermodynamic profiles in TC environments. It is found that convective echoes are affected by a stratiform region-induced stable layer, which enhances our understanding of the general durability of such 0°C thermodynamic profiles. In addition, the results show that in TC environments the most frequent type of raining feature are those that appear at and just above 0°C. Considering the difficulty in parameterizing subscale TC-related features in cumulus and microphysical schemes, these types of insights should help us more accurately forecast many TC-related processes. Due to a lack of comprehensive TC cloud observations, in this study it was necessary to analyze precipitating features as measured by TRMM's precipitation radar. Such a large data set would be possible with few, if any, other methods. Future studies will be conducted to analyze echo distributions in other parts of the globe, as the results would likely tell us much of region-specific tropical interactions. Considering the important role clouds play in our climate system and the subtle cloud-related processes that accompany TC intensity change, the findings from this paper provide an important quantitative view of the distribution and characteristics of TC and tropical precipitation features in the west Pacific.

[37] **Acknowledgments.** We would like to thank the National Science Foundation in the U.S. and the Japan Society for the Promotion of Science for making the first author's visit to the Atmosphere and Ocean Research Institute at the University of Tokyo possible. This project began there as part of the NSF's East Asia and Pacific Summer Institutes program. The first and last authors were supported by the Office of Naval Research (ONR). Helpful discussions with Edward Zipser regarding the manuscript are also greatly appreciated, as were the very useful comments of two reviewers.

References

- Awaka, J., T. Iguchi, H. Kumagai, and K. Okamoto (1997), Rain type classification algorithm for TRMM precipitation radar, paper presented at 1997 International Geoscience and Remote Sensing Symposium, IEEE, Singapore, Japan.
- Cecil, D. J., S. J. Goodman, D. J. Boccippio, E. J. Zipser, and S. W. Nesbitt (2005), Three years of TRMM precipitation features. Part I: Radar,

- radiometric, and lightning characteristics, *Mon. Weather Rev.*, *133*, 543–566, doi:10.1175/MWR-2876.1.
- Cheng, C.-P., and R. A. Houze (1979), The distribution of convective and mesoscale precipitation in GATE radar echo patterns, *Mon. Weather Rev.*, *107*, 1370–1381, doi:10.1175/1520-0493(1979)107<1370:TDO-CAM>2.0.CO;2.
- Ferrier, B. S., and R. A. Houze (1989), One-dimensional time-dependent modeling of GATE cumulonimbus convection, *J. Atmos. Sci.*, *46*, 330–352, doi:10.1175/1520-0469(1989)046<0330:ODTDMO>2.0.CO;2.
- Franklin, J. L., M. L. Black, and K. Valde (2003), GPS dropwindsonde wind profiles in hurricanes and their operational implications, *Weather Forecast.*, *18*, 32–44, doi:10.1175/1520-0434(2003)018<0032:GDWPIH>2.0.CO;2.
- Halverson, J. B., et al. (2007), NASA's Tropical Cloud Systems and Processes Experiment: Investigating tropical cyclogenesis and hurricane intensity change, *Bull. Am. Meteorol. Soc.*, *88*, 867–882, doi:10.1175/BAMS-88-6-867.
- Heymsfield, G. M., L. Tian, A. J. Heymsfield, L. Li, and S. Guimond (2010), Characteristics of deep tropical and subtropical convection from a nadir-viewing high-altitude airborne Doppler radar, *J. Atmos. Sci.*, *67*, 285–308, doi:10.1175/2009JAS3132.1.
- Houze, R. A. (2010), Clouds in tropical cyclones, *Mon. Weather Rev.*, *138*, 293–344, doi:10.1175/2009MWR2989.
- Houze, R. A., and C.-P. Cheng (1977), Radar characteristics of tropical convection observed during GATE: Mean properties and trends over the summer season, *Mon. Weather Rev.*, *105*, 964–980, doi:10.1175/1520-0493(1977)105<0964:RCOTCO>2.0.CO;2.
- Iguchi, T., T. Kozu, R. Meneghini, J. Awaka, and K. Okamoto (2000), Rain-profiling algorithm for the TRMM precipitation radar, *J. Appl. Meteorol.*, *39*, 2038–2052, doi:10.1175/1520-0450(2001)040<2038:RPAFTT>2.0.CO;2.
- Jensen, M. P., and A. D. Del Genio (2006), Factors limiting convective cloud-top height at the ARM Nauru Island climate research facility, *J. Clim.*, *19*, 2105–2117, doi:10.1175/JCLI3722.1.
- Jiang, H., C. Liu, and E. J. Zipser (2011), A TRMM-based tropical cyclone cloud and precipitation database, *J. Appl. Meteorol. Climatol.*, *50*, 1255–1274, doi:10.1175/2011JAMC2662.
- Johnson, R. H., P. E. Ciesielski, and K. A. Hart (1996), Tropical inversions near the 0°C level, *J. Atmos. Sci.*, *53*, 1838–1855, doi:10.1175/1520-0469(1996)053<1838:TINTL>2.0.CO;2.
- Johnson, R. H., T. M. Rickenbach, S. A. Rutledge, P. E. Ciesielski, and W. H. Schubert (1999), Trimodal characteristics of tropical convection, *J. Clim.*, *12*, 2397–2418, doi:10.1175/1520-0442(1999)012<2397:TCOTC>2.0.CO;2.
- Kozu, T., T. Kawanishi, H. Kuroiwa, M. Kojima, K. Oikawa, H. Kumagai, K. Okamoto, M. Okumura, H. Nakatsuka, and K. Nishikawa (2001), Development of precipitating radar onboard the Tropical Rainfall Measuring Mission (TRMM) satellite, *IEEE Trans. Geosci. Remote Sens.*, *39*, 102–116, doi:10.1109/36.898669.
- Kummerow, C., W. Barnes, T. Kozu, J. Shiue, and J. Simpson (1998), The Tropical Rainfall Measuring Mission (TRMM) sensor package, *J. Atmos. Oceanic Technol.*, *15*, 809–817, doi:10.1175/1520-0426(1998)015<0809:TTRMMT>2.0.CO;2.
- Leary, C. A., and R. A. Houze (1979), Melting and evaporation of hydrometeors in precipitation from the anvil clouds of deep tropical convection, *J. Atmos. Sci.*, *36*, 669–679, doi:10.1175/1520-0469(1979)036<0669:MAEOHI>2.0.CO;2.
- Liu, C., E. J. Zipser, and S. W. Nesbitt (2007), Global distribution of tropical deep convection: Different perspectives from TRMM infrared and radar data, *J. Clim.*, *20*, 489–503, doi:10.1175/JCLI4023.1.
- Liu, C., E. J. Zipser, D. J. Cecil, S. W. Nesbitt, and S. Sherwood (2008), A cloud and precipitation feature database from 9 years of TRMM observations, *J. Appl. Meteorol. Climatol.*, *47*, 2712–2728, doi:10.1175/2008JAMC1890.1.
- Nesbitt, S. W., E. J. Zipser, and D. J. Cecil (2000), A census of precipitation features in the tropics using TRMM: Radar, ice scattering, and lightning observations, *J. Clim.*, *13*, 4087–4106, doi:10.1175/1520-0442(2000)013<4087:ACOPFI>2.0.CO;2.
- Randall, D. A., and G. J. Huffman (1980), A stochastic model of cumulus clumping, *J. Atmos. Sci.*, *37*, 2068–2078, doi:10.1175/1520-0469(1980)037<2068:ASMOCC>2.0.CO;2.
- Rickenbach, T. M., and S. A. Rutledge (1998), Convection in TOGA COARE: Horizontal scale, morphology, and rainfall production, *J. Atmos. Sci.*, *55*, 2715–2729, doi:10.1175/1520-0469(1998)055<2715:CITCHS>2.0.CO;2.
- Rogers, R., et al. (2006), The Intensity Forecasting Experiment: A NOAA multiyear field program for improving tropical cyclone intensity forecasts, *Bull. Am. Meteorol. Soc.*, *87*, 1523–1537, doi:10.1175/BAMS-87-11-1523.

- Schubert, W. H. (1976), Experiments with Lilly's cloud-topped mixed layer model, *J. Atmos. Sci.*, *33*, 436–446, doi:10.1175/1520-0469(1976)033<0436:EWLCTM>2.0.CO;2.
- Schumacher, C., and R. A. Houze Jr. (2003a), Stratiform rain in the tropics as seen by the TRMM precipitation radar, *J. Clim.*, *16*, 1739–1756, doi:10.1175/1520-0442(2003)016<1739:SRITTA>2.0.CO;2.
- Schumacher, C., and R. A. Houze Jr. (2003b), The TRMM precipitation radar's view of shallow, isolated rain, *J. Appl. Meteorol.*, *42*, 1519–1524, doi:10.1175/1520-0450(2003)042<1519:TTPRVO>2.0.CO;2.
- Sherwood, S. C. (1999), Convective precursors and predictability in the tropical western Pacific, *Mon. Weather Rev.*, *127*, 2977–2991, doi:10.1175/1520-0493(1999)127<2977:CPAPIT>2.0.CO;2.
- Smith, E. A., F. J. Turk, M. R. Farrar, A. Mugnai, and X. Xiang (1997), Estimating 13.8-GHz path-integrated attenuation from 10.7-GHz brightness temperatures for the TRMM combined PR-TMI precipitation algorithm, *J. Appl. Meteorol.*, *36*, 365–388, doi:10.1175/1520-0450(1997)036<0365:EGPIAF>2.0.CO;2.
- Steiner, M., R. A. Houze, and S. Yuter (1995), Climatological characterization of three-dimensional storm structure from operational radar and rain gauge data, *J. Appl. Meteorol.*, *34*, 1978–2007, doi:10.1175/1520-0450(1995)034<1978:CCOTDS>2.0.CO;2.
- Takayabu, Y. N., J. Yokomori, and K. Yoneyama (2006), A diagnostic study on interactions between atmospheric thermodynamic structure and cumulus convection over the tropical western Pacific Ocean and over the Indochina peninsula, *J. Meteorol. Soc. Jpn.*, *84A*, 151–169, doi:10.2151/jmsj.84A.151.
- Takayabu, Y. N., S. Shige, W.-K. Tao, N. Hirota (2010), Shallow and deep latent heating modes over tropical oceans observed with TRMM PR spectral latent heating data, *J. Clim.*, *23*, 2030–2046, doi:10.1175/2009JCLI3110.1.
- Takemi, T., O. Hirayama, and C. Liu (2004), Factors responsible for the vertical development of tropical oceanic cumulus convection, *Geophys. Res. Lett.*, *31*, L11109, doi:10.1029/2004GL020225.
- Taylor, G. R., and M. B. Baker (1991), Entrainment and detrainment in cumulus clouds, *J. Atmos. Sci.*, *48*, 112–121, doi:10.1175/1520-0469(1991)048<0112:EADICC>2.0.CO;2.
- Wang, Y., and C.-C. Wu (2004), Current understanding of tropical cyclone structure and intensity changes—A review, *Meteorol. Atmos. Phys.*, *87*, 257–278, doi:10.1007/s00703-003-0055-6.
- Warner, C., J. Simpson, G. Van Helvoirt, D. W. Martin, D. Suchman, and G. L. Austin (1980), Deep convection on day 261 of GATE, *Mon. Weather Rev.*, *108*, 169–194, doi:10.1175/1520-0493(1980)108<0169:DCODOG>2.0.CO;2.
- Yanai, M., S. Ebsensen, and J.-H. Chu (1973), Determination of bulk properties of tropical cloud clusters from large-scale heat and moisture budgets, *J. Atmos. Sci.*, *30*, 611–627, doi:10.1175/1520-0469(1973)030<0611:DOBPOT>2.0.CO;2.
- Yanai, M., J.-H. Chu, T. E. Stark, and T. Nitta (1976), Response of deep and shallow tropical maritime cumuli to large-scale processes, *J. Atmos. Sci.*, *33*, 976–991, doi:10.1175/1520-0469(1976)033<0976:RODAST>2.0.CO;2.
- Yokoyama, C., and Y. N. Takayabu (2008), A statistical study on rain characteristics of tropical cyclones using TRMM satellite data, *Mon. Weather Rev.*, *136*, 3848–3862, doi:10.1175/2008MWR2408.1.
- Yokoyama, C., and Y. N. Takayabu (2012), Relationships between rain characteristics and environment. Part I: TRMM precipitation feature and the large-scale environment over the tropical Pacific, *Mon. Weather Rev.*, doi:10.1175/MWR-D-11-00252.1, in press.
- Zuidema, P. (1998), The 600–800mb minimum in tropical cloudiness observed during TOGA COARE, *J. Atmos. Sci.*, *55*, 2220–2228, doi:10.1175/1520-0469(1998)055<2220:TMMITC>2.0.CO;2.